Implementation of a closed-loop structural control system using wireless sensor networks

J. P. Lynch[a*], Y. Wang[b], R. A. Swartz[a], K. C. Lu[c], C. H. Loh[c]

[a]*Department of Civil and Environmental Engineering, University of Michigan, Ann Arbor, MI, 48109-2125*
[b]*Department of Civil and Environmental Engineering, Stanford University, Stanford, CA, 94305*
[c]*Department of Civil Engineering, National Taiwan University, Taipei, Taiwan, R.O.C.*

SUMMARY

Wireless sensor networks have rapidly matured in recent years to offer data acquisition capabilities on par with those of traditional tethered data acquisition systems. Entire structural monitoring systems assembled from wireless sensors have proven to be low-cost, easy to install and accurate. However, the functionality of wireless sensors can be further extended to include actuation capabilities. Wireless sensors capable of actuating a structure could serve as building blocks of future generations of structural control systems. In this study, a wireless sensor prototype capable of data acquisition, computational analysis and actuation is proposed for use in a real-time structural control system. The performance of a wireless control system is illustrated using a full-scale structure controlled by a semi-active magnetorheological (MR) damper and a network of wireless sensors. One wireless sensor is designated as a controller that automates the task of collecting state data, calculating control forces, and issuing commands to the MR damper, all in real-time. Additional wireless sensors are installed to measure the acceleration and velocity response of each system degree-of-freedom. Base motion is applied to the structure to simulate seismic excitations while the wireless control system mitigates the inter-story drift and relative acceleration response of the structure. An optimal linear quadratic regulation (LQR) solution is formulated for embedment within the computational cores of the wireless sensors.

KEY WORDS: Structural control; Wireless sensors; Embedded computing; Magnetorheological dampers

1. INTRODUCTION

Recent natural catastrophes have revealed the vulnerabilities of critical civil infrastructure systems (bridges, buildings, tunnels, dams) exposed to earthquakes, hurricanes, and typhoons. To mitigate structural responses resulting from dynamic loads, feedback control systems have been proposed by Yao

* Corresponding author.
E-mail address: jerlynch@umich.edu (Assistant Professor Jerome P. Lynch)

[1] for installation in civil structures. Since that time, feedback control systems have been widely adopted with over 50 buildings and 20 long-span bridges in Asia currently employing feedback control [2]. Early structural control systems proposed for civil structures employed large actuators for the direct application of control forces. While active control systems were successful at mitigating structural responses to wind loads, force capacities of actuators often saturate during large seismic events thereby limiting their effectiveness. In response to this limitation, the concept of semi-active structural control was proposed. Unlike the actuators employed in active control systems, semi-active control devices are designed to develop internal structural forces by changes to the damping and stiffness properties of the structure. Examples of semi-active devices include, but are not limited to: active variable stiffness (AVS) devices [3], semi-active hydraulic dampers (SHD) [4], electrorheological (ER) dampers [5], and magnetorheological (MR) dampers [6]. A benefit of developing control forces in a structure indirectly is that semi-active control devices consume an order of magnitude less power than actuators associated with active control systems [7]. In addition to inherent energy efficiencies, semi-active control devices are also compact and low-cost. These attractive attributes encourage the use of large numbers of semi-active control devices in a single structure; examples include 88 SHD devices in the Shiodome Tower, Tokyo and over 350 SHD devices installed in the Mori Tower, Tokyo [2].

As recent installations suggest, future semi-active control systems will continue to be defined by ever greater nodal densities. As structural control systems grow in size, the design and installation complexities of the systems increase in tandem. For example, structural control systems currently employ extensive lengths of coaxial wire to accommodate communication between sensors, actuators and a centralized controller. As nodal densities increase, more coaxial wire is needed for communication. In 2002, the installation of coaxial wire between sensors and a central data repository has been cited to cost as high as a few thousand dollars per sensor channel [8]. As a result, the benefit derived from additional control devices are eroded by the high installation costs associated with increasing lengths of coaxial wire. To eradicate the high cost of a wired control system, the use of wireless communications is proposed for systems defined by high nodal densities.

Other researchers have previously explored wireless communications for adoption in feedback control systems. Unlike current control systems that have dedicated coaxial wires between sensors, actuators and the centralized controller, a control system adopting wireless communications requires sensors and controllers to share a common wireless medium for communication. When a closed-loop control system is implemented using a common communication medium (wired or wireless), network quality strongly influences the performance of the control solution. Specifically, time delays governed by deterministic and stochastic processes are often introduced by the network. Lian, *et al.* [9] proposes the use of network protocols that guarantee deterministic transmission times between transmitting and receiving nodes so that delays can be accounted for by the control solution. However, stochastic delays sometimes can not be avoided and are difficult to account for *a priori*. Specific to wireless networks, multiple researchers have begun to explore real-time closed-loop control using wireless sensors. Eker, *et al.* [10] explores the implementation of a linear quadratic regulation (LQR) control solution using a wireless controller that communicates using the Bluetooth wireless communication protocol. Randomly varying delays within the wireless communication channel are compensated for in the design of the LQR controller using a compensation technique proposed by Nilsson, *et al.* [11]. Ploplys, *et al.* [12] implements a closed-loop control solution for an inverted pendulum system using a wireless sensor network communicating upon the IEEE 802.11b communication standard. To ensure timely delivery of data packets, the User Datagram Protocol (UDP) is adopted to provide fast sample rates and to reduce network congestion.

In this study, a real-time structural control system for civil structures is proposed using wireless sensor networks. As a fundamental building block of the control system, a wireless sensor prototype is

designed to provide the functionality required for real-time control including data collection, computation and actuation. The hardware design of the wireless sensor described herein is largely based upon a wireless sensor previously proposed for infrastructure monitoring [13]. The actuation interface of the modified wireless sensor is designed to output an analog voltage signal to command semi-active control devices in real-time. One challenge associated with wireless communications is to ensure the reliable delivery of data in the network. To address this challenge, a reliable wireless communication protocol is proposed based upon a time division multiple access (TDMA) communication scheme. The feasibility of a wireless control system is validated using a full-scale three-story steel structure excited by seismic ground motions. A 20 kN MR damper is installed at the base of the structure for mitigation of structural responses (inter-story drifts and floor accelerations). The bounded input-bounded output (BIBO) stability property of semi-active dampers protect the test structure from becoming unstable should the wireless control system perform poorly. Two control system architectures are implement; one architecture adopts velocity transducers while the second adopts accelerometers. The performance of the wireless control system will be quantified by comparing the closed-loop control performance to utilizing the MR damper in a passive configuration. In addition, the wireless control system performance is also compared to that of a control system implemented using a wired laboratory data acquisition system. As a result of computational and communication overhead, the wireless control system is operated at a 12.5 sample rate while the baseline tethered control system operates at 200 Hz. The wireless control system is shown to be both effective in reducing structural responses and reliable in the wireless delivery of state data at each time step.

2. PROTOTYPE WIRELESS SENSOR FOR MONITORING AND CONTROL

Numerous commercial and academic wireless sensors have been proposed for monitoring civil structures [14]. The hardware design of all of these wireless sensors can be divided into four functional components: sensing interface, computational core, wireless communication channel and actuation interface. The sensing interface allows a variety of sensing transducers to be interfaced to a wireless sensor. A core element of the sensing interface is an analog-to-digital converter (ADC) which converts analog sensor signals to binary representations. After data is collected and digitized by the sensing interface, it is passed to the computational core where data is stored, analyzed and readied for communication. The third functional component is the wireless communication channel which offers each wireless sensor connectivity to the remainder of the wireless sensor network. A large majority of the wireless sensors proposed for structural monitoring integrate these first three functional components. However, recent wireless sensor designs have begun to include an actuation interface as a forth functional component [15]. This study will modify the design of an existing wireless sensor prototype to accommodate an actuation interface for use in a control system [13].

The architectural design of the wireless sensor prototype is presented in Figure 1(a). The sensing interface is designed around the Texas Instruments ADS8341 ADC which offers a 16-bit conversion resolution and 4 sensing channels. The sensing interface is capable of digitizing any analog signal in the 0 – 5 V range at sample rates as high as 100 kHz. The computational core consists of a low-power 8-bit microcontroller and external random access memory (RAM). The Atmel ATmega128 microcontroller is selected for its abundance of on-board read only memory (128 kB) where embedded software is stored for execution by the wireless sensor. However, the chip lacks sufficient RAM (4 kB) which is necessary for the storage of measurement data. In response to this limitation, the computational core is designed with external static RAM (SRAM) (Cypress CY62128B) offering 128 kB of additional memory. The wireless

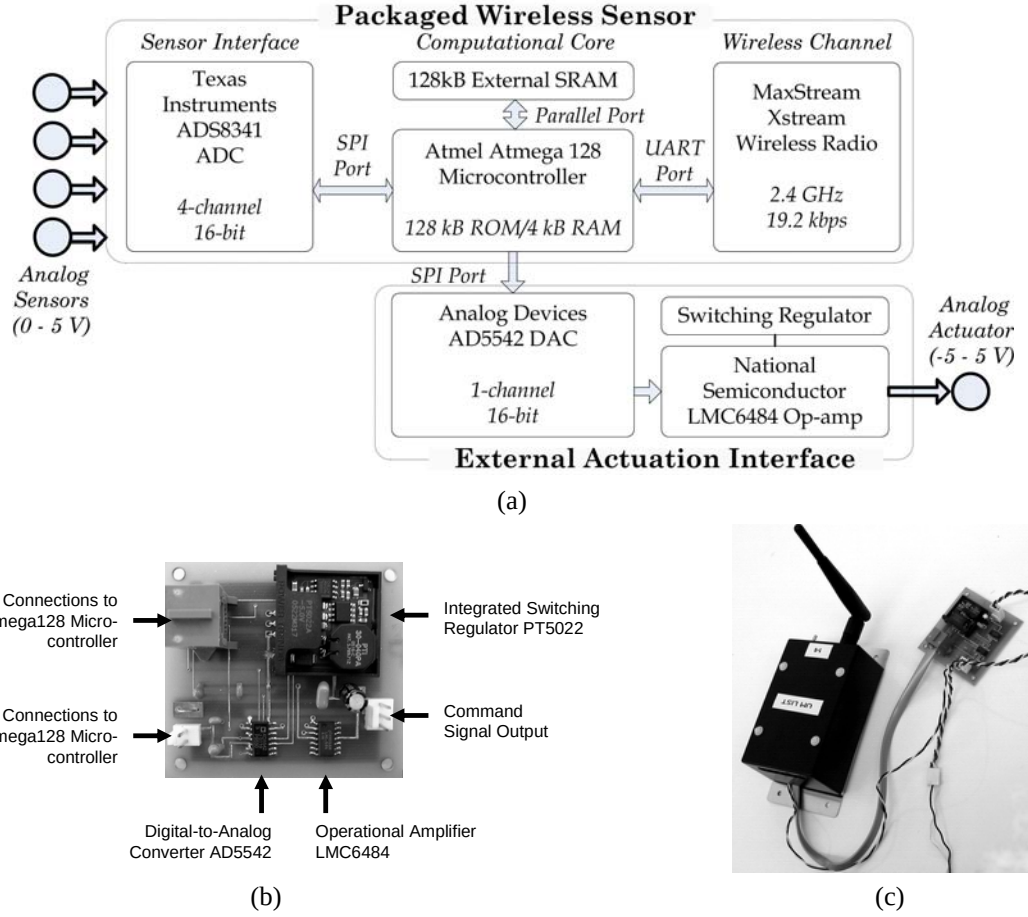

Figure 1. (a) Architectural overview of a wireless sensor prototype for structural control; (b) stand-alone actuation interface circuit; (c) fully assembled wireless sensor with external actuation interface attached

communication channel is serviced by the MaxStream XStream wireless modem; the XStream operates on the 2.4 GHz radio band and has a communication speed of 19.2 kbps. The radio is selected for its optimal balance between power consumption and communication range. Line-of-sight communication distances of up to 11 km can be attained with the wireless modem. The power consumption of the wireless radio is 750 mW when transmitting, 400 mW when receiving and 0.13 mW when in standby (neither transmitting nor receiving). The sensing interface, computational core and wireless communication channel hardware components are integrated upon two printed circuit boards and packaged in a hardened container (6.4 *x* 10 *x* 8 cm^3) for use in the harsh field environment. To power the wireless sensor, 5 AA lithium-ion batteries are included in the hardened container. If the wireless sensor is continuously powered on, the life expectancy of the sensor is roughly 30 hours; duty cycle usage strategies can extend its operational life to the order of years.

The actuation interface is designed upon its own two-layer printed circuit board and externally attached to the wireless sensor. The core hardware component integrated in the actuation interface is a digital-to-analog converter (DAC) which receives binary numbers from the microcontroller and converts them to zero-order hold analog voltage signals. The single-channel 16-bit Analog Devices AD5542

DAC, capable of a maximum sample rate of 1 MHz, is selected. The wireless sensor provides a 5 V power supply for the AD5542 effectively allowing the DAC to output analog voltage signals from 0 to 5 V. An additional op-amp (National Semiconductor LMC6484) is included to broaden the 0 to 5 V output range of the DAC to -5 to 5 V. To provide negative voltage outputs, the op-amp must be powered with a 5 and -5 V voltage supply. The 5 V supply is provided by the wireless sensor; the -5 V supply is generated by a Texas Instruments PT5022 switching regulator which converts the wireless sensor regulated 5 V power supply to a -5 V supply. Figure 1(b) provides a picture of the stand-alone actuation interface circuit while Figure 1(c) presents a fully assembled wireless sensor capable of actuation.

3. SEMI-ACTIVELY CONTROLLED STEEL STRUCTURE

3.1. Full-scale validation structure excited by base motions

In this study, a full-scale steel structure is constructed upon a large shaking table (5 by 5 m footprint) at the National Center for Research on Earthquake Engineering (NCREE), Taiwan. The shaking table can be commanded in 6 degrees-of-freedom so that a realistic seismic loading can be applied to the base of the structure. The shaking table is capable of exerting motions between 0.1 and 50 Hz with a maximum acceleration and inertial force of 9.8 m/s^2 and 220 kN, respectively. The steel structure is a single bay, three-story building frame constructed from I-beam (H150x150x7x10) steel elements. The height of each floor is 3 m (total structure height is 9 m) and the floor area is 3 by 2 m. The floors are designed as rigid diaphragms that do not deform when the structure is excited by base motion; rather, the lateral response of the structure is through shear deformation of each floor's 4 columns. Additional mass is applied to each floor to ensure a total mass of 6,000 kg is associated with each lateral degree-of-freedom. Experimental testing on the structure reveals the structure to be lightly damped with a damping ratio of roughly 3%. Figure 2(b) provides a top perspective view of the test structure mounted to the NCREE shaking table.

3.2. Semi-active magnetorheological damper

A magnetorheological (MR) damper, whose damping coefficient can be changed in real-time, is installed at the base of the steel structure. The damper is installed within a steel V-brace to transfer the damper force to the first floor of the structure. The MR damper piston is filled with a silicon oil saturated with magnetically polarizable particles. A coil tightly wrapped around the piston cylinder is used to induce a magnetic field in the damper piston. When no current is applied to the coil, the oil freely flows as a viscous fluid; when high currents are applied, particles suspended in the oil align resulting in a semi-solid piston material whose yield strength is proportional to the coil current. The MR damper installed in the test structure is capable of a maximum control force of 20 kN, stroke of 10.8 cm, and can be controlled by a simple command voltage ranging from 0 to 1 V [16]. To power the MR damper, a separate 24 V laboratory power supply is employed; the power supply receives the 0 to 1 V command signal and converts the voltage command signal to an electrical current (0 to 2 A) that is then delivered to the damper coil. The MR damper, including the load cell installed in series, is pictured in Figure 2(c).

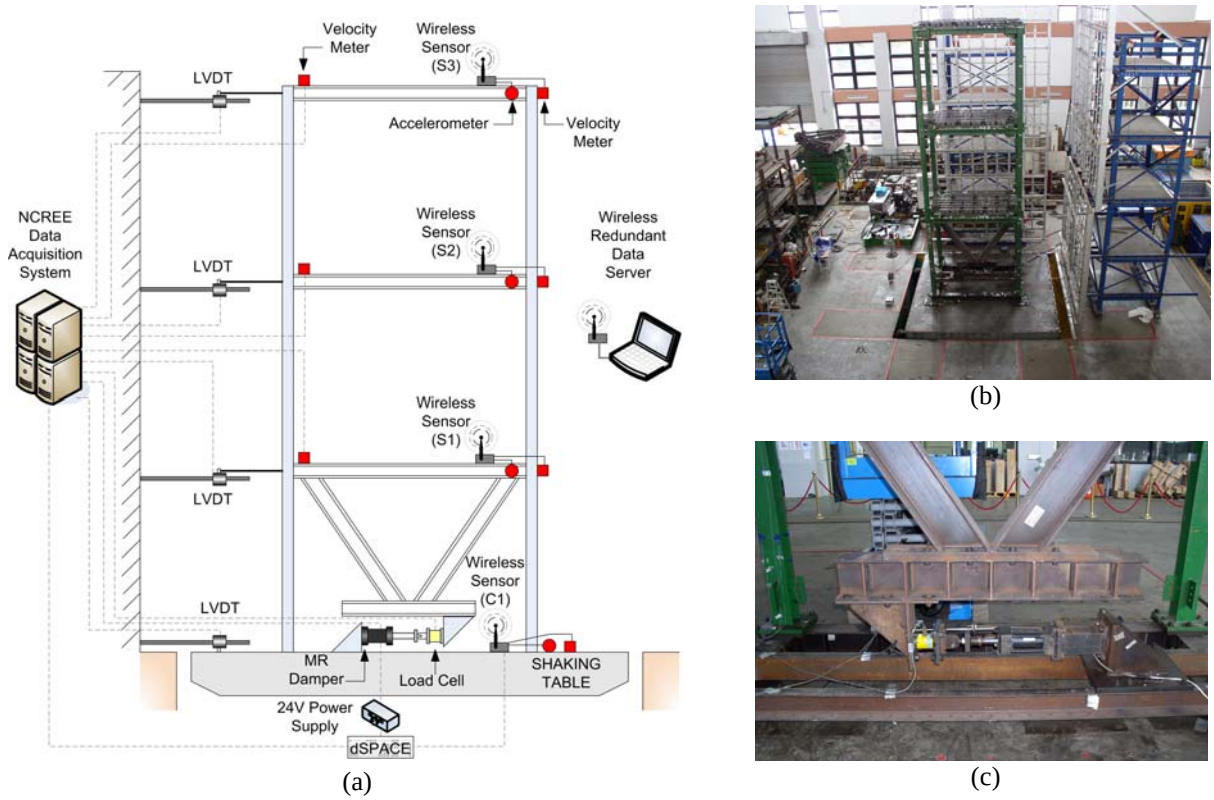

Figure 2. (a) Overview of the 3-story test structure and its instrumentation; (b) completed structure mounted to the NCREE shaking table; (c) close-up view of the MR damper at the structure base.

MR dampers are nonlinear devices that must be properly modeled before they can be employed within a structural control system. A number of parametric models that fully describe the force-velocity relationships of MR dampers have been formulated [6]. One such parametric model is the Bouc-Wen model, whose computational tractability and model flexibility are attractive features. For the 20 kN MR damper used in this study, a modified Bouc-Wen model has been proposed by Lin, *et al.* [16]. The force in the MR damper, F, results from an equivalent viscous damper with the addition of a hysteretic restoring force, z.

$$F(t) = C(V)\dot{x}(t) + z(t) \tag{1}$$

Here, the damping coefficient, C, is controllable by the damper command voltage, V. The hysteretic restoring force, z, is defined by a Bouc-Wen model whose parametric constants are A, β, γ, and n:

$$\dot{z}(t) = A\dot{x}(t) + \gamma\dot{x}(t)\left|z(t)\right|^{n} + \beta\left|\dot{x}(t)\right|\left|z(t)\right|^{n-1} z(t) \tag{2}$$

where, $\dot{x}(t)$, is the shaft velocity of the damper. The Bouc-Wen model can be modified to include additional terms with the model order, N, introduced as an additional parametric variable [17]:

$$\dot{z}(t) = A\dot{x}(t) + \sum_{n=1}^{N} a_n \left[\gamma \dot{x}(t)|z(t)|^n + \beta|\dot{x}(t)||z(t)|^{n-1} z(t)\right] \tag{3}$$

For most mechanical systems exhibiting hysteretic behavior, a model order up to $N = 3$ is sufficient [18]. However, a modified Bouc-Wen model of order $N = 2$ is considered in this study. The modified Bouc-Wen model can be written in discrete-time at time step, k (where $t = k\Delta t$):

$$\begin{aligned} &z(k) - z(k-1) = \Delta t\left[\mathbf{\Phi}(k-1)^T \mathbf{\Theta}\right] \\ &\mathbf{\Theta}^T = \{\theta_1 \quad \theta_2 \quad \theta_3 \quad \theta_4 \quad \theta_5\} \\ &\mathbf{\Phi}(k)^T = \left\{\dot{x}(k) \quad |\dot{x}(k)|z(k) \quad \dot{x}(k)|z(k)| \quad |\dot{x}(k)||z(k)|z(k) \quad \dot{x}(k)|z(k)|^2\right\} \end{aligned} \tag{4}$$

The parametric variables, θ_i, of the modified Bouc-Wen model can be determined by using standard model fitting techniques applied to experimental data collected from the MR damper. To fully characterize the MR damper properties, the damper is attached to a displacement-controlled actuator that can apply displacement time-histories. In addition, a load cell is attached to the other end of the damper to measure the MR damper reaction force. Random displacement time-histories are applied to the MR damper to generate a complete set of force-velocity time histories corresponding to constant damper voltages spanning from 0 to 1 V. Lin, *et al.* [16] describe the use of a gradient projection law for adaptive estimation of the parametric variables using the force-velocity time histories collected under random displacements. It should be noted that the parametric model variables, θ_i, are specified for each voltage level applied. The MR damper test is repeated for various command voltages, V, to derive an MR damper force-velocity relationship when the damper command voltage varies:

$$\begin{aligned} &F(k) = 0.0083V + 0.005 + z(k) \\ &z(k) = z(k-1) + \Delta t\left[\mathbf{\Phi}(k-1)^T \mathbf{\Theta}\right] \\ &\theta_1(V) = -13.3V^3 + 23.0V^2 + 1.0V - 1.1 \\ &\theta_2(V) = -161.6V^2 - 88.7V - 389.3 \\ &\theta_3(V) = -5.0V^2 - 169.2V - 160.4 \\ &\theta_4(V) = -6433V^2 - 80282V - 7757 \\ &\theta_5(V) = 0.35V^2 - 6.8V - 0.32 \end{aligned} \tag{5}$$

The parametric model is tuned using the units of m/s for the damper shaft velocity and MN for the MR damper force.

3.3. Sensor instrumentation of the test structure

Two redundant data acquisition systems are installed within the steel structure to conduct real-time feedback control during seismic excitation. The first data acquisition system is entirely wireless and is assembled from a network of wireless sensor prototypes. The second system consists of a tethered data acquisition system permanently installed for testing and controlling specimens on the NCREE facility shaking table.

As shown in Figure 2(a), the wireless control system consists of one wireless sensor installed upon each level of the structure (4 wireless sensors in total). The wireless sensors installed on the first, second and third floors are denoted as S1, S2, and S3, respectively. These wireless sensors are responsible for measuring the lateral response of each floor using two sensing transducers interfaced. The first transducer is the Tokyo Sokushin VSE-15-AM servo velocity meter. The VSE-15 is capable of measuring velocities within a 0.1 to 70 Hz range and up to a maximum magnitude of 1 m/s. The sensitivity constant of the sensor is 10 V/(m/s) and outputs its measurement upon a -10 to 10 V output signal. To interface to the wireless sensors, a signal condition circuit is designed to shift the zero mean sensor output to 2.5 V and to de-amplify the output by a factor of 4. The second transducer installed on each floor is the Crossbow CXL02 microelectromechanical system (MEMS) accelerometer. This low-cost accelerometer can measure accelerations from 0 to 50 Hz with a maximum magnitude of 19.6 m/s^2. The accelerometer, with a sensitivity of 0.102 $V/(m/s^2)$, has a voltage output range from 0 to 5 V.

The fourth wireless sensor, denoted as C1, is mounted to the surface of the shaking table in the vicinity of the MR damper. This wireless sensor is responsible for measuring the base excitation in addition to determining control forces and issuing command signals to the MR damper. To measure the base excitation, a Tokyo Sokushin VSE-15 velocity meter and Crossbow CXL02 accelerometer are interfaced. The actuation channel of wireless sensor C1 is connected to a dSPACE real-time input/output board that controls the operation of the MR damper power supply. To initiate the operation of the wireless control system and to log data wirelessly transmitted by the wireless sensors during testing, a laptop computer is installed in the lab roughly 100 m from the test structure. A 2.4 GHz XStream wireless radio is interfaced to the laptop computer for recording the flow of data in the network of wireless sensors.

A tethered data acquisition system is used as a performance baseline to which the wireless control system can be compared. The resolution of the laboratory data acquisition system is 16-bits and offers a total of 128 sensor channels. To obtain an accurate measurement of the state of the system during excitation, both velocity meters and linear variable displacement transducers (LVDT) are installed at each floor to measure the absolute velocity and displacement of the structure. A second set of Tokyo Sokushin VSE-15-AM velocity meters are installed adjacent to the velocity meters interfaced to the wireless monitoring system. To measure the absolute displacement of each degree-of-freedom of the structure, Temposonics II position sensors with a range of 400 mm and a displacement resolution of 25 μm are installed between each floor and a static reference frame constructed to the side of the shaking table. To measure the damper response, a Temposonics II position sensor is also mounted to the damper to measure shaft displacements while a 50 kN load cell is installed between the damper and the steel bracing system.

4. WIRELESS CONTROL SYSTEM ARCHITECTURE

A centralized system architecture is proposed for the wireless control system with wireless sensor C1 placed at the center of the system. Wireless sensor C1 is responsible for the collection of structural response data (velocity or acceleration) from wireless sensors S1, S2 and S3. Wireless sensors S1, S2 and S3 are responsible only for the measurement of the structural response when queried by wireless sensor C1. Upon receipt of response data, wireless sensor C1 is also given the responsibility to determine a control force to be applied to the structure using the MR damper. After calculating the optimal control force, the wireless sensor then issues a command signal to the MR damper.

Two centralized control solutions will be embedded in wireless sensor C1, depending upon the sensing transducer interfaced to the wireless control system. When servo velocity meters are interfaced to

the wireless sensors for measurement of the structural velocity, a velocity feedback control solution is employed. In contrast, if accelerometers are used in lieu of velocity meters, then a steady-state Kalman filter is implemented for estimation of the dynamic state of the structure for full-state feedback control. In both control solutions, linear quadratic regulation is employed.

4.1. Centralized linear quadratic regulation control

A commonly employed centralized control solution for reducing the dynamic response of civil structures is the linear quadratic regulator (LQR) [19]. The LQR control solution is optimal since it minimizes a desired response parameter, $\mathbf{y}(t)$, by exerting a minimal amount of control effort. The equation of motion of a multiple degree-of-freedom structure, defined by n degrees-of-freedom, is formulated in state-space form.

$$\dot{\mathbf{z}}(t) = \mathbf{A}\mathbf{z}(t) + \mathbf{B}\mathbf{u}(t) + \mathbf{H}\mathbf{f}(t)$$

$$\mathbf{z}(t) = \begin{Bmatrix} \mathbf{x}(t) \\ \dot{\mathbf{x}}(t) \end{Bmatrix} \quad \mathbf{A} = \begin{bmatrix} \mathbf{0} & \mathbf{I} \\ -\mathbf{M}^{-1}\mathbf{K} & -\mathbf{M}^{-1}\mathbf{C}_{damp} \end{bmatrix} \tag{6}$$

The state response of the structure, $\mathbf{z}$, due to applied external loading, $\mathbf{f}$, is a vector containing the lateral displacement, $\mathbf{x}$, and velocity, $\dot{\mathbf{x}}$, of each floor relative to the structure base. The properties of the structure, namely mass, stiffness, and damping, $\mathbf{M}$, $\mathbf{K}$ and $\mathbf{C}_{damp}$, are used to derive the system matrix, $\mathbf{A}$. If the structure is controlled, the control forces, $\mathbf{u}$, applied by the control system are included in the state-space equation of motion. The locations of the external system loading, $\mathbf{f}$, and the internal control forces, $\mathbf{u}$, are established by the location matrices $\mathbf{H}$ and $\mathbf{B}$, respectively. The structural response parameter to be minimized by the LQR control solution is written as a linear function of the state response:

$$\mathbf{y}(t) = \mathbf{C}\mathbf{z}(t) \tag{7}$$

The LQR control solution derives an optimal state trajectory of the state response $\mathbf{z}$ by simultaneously minimizing the response parameter, $\mathbf{y}$, and the control effort, $\mathbf{u}$. The optimal state trajectory is determined by minimization of a scalar cost function, J, over the time trajectory of the system:

$$J = \int_0^{t_f} \mathbf{y}^T\mathbf{y} + \mathbf{u}^T\mathbf{R}\mathbf{u} \tag{8}$$

A weighting matrix, $\mathbf{R}$, is included in the scalar cost function so that the importance of minimizing the control effort relative to minimizing the structural response parameter can be explicitly expressed. Minimization of the scalar cost function, J, by Lagrangian methods results in a constant gain matrix, $\mathbf{G}$, that when multiplied by the state of system, $\mathbf{z}$, provides the optimal control forces, $\mathbf{u}$:

$$\mathbf{u}(t) = \mathbf{G}\mathbf{z}(t) \tag{9}$$

For the three-story steel structure, the system is modeled as a lumped mass shear-structure. The structural response is defined by the deflection of each floor relative to the base of the structure. The lumped mass matrix and the stiffness matrix are formulated for the three-story steel structure:

$$\mathbf{M} = \begin{bmatrix} 6 & 0 & 0 \\ 0 & 6 & 0 \\ 0 & 0 & 6 \end{bmatrix} x10^3 kg \quad \text{and} \quad \mathbf{K} = \begin{bmatrix} 4.2 & -2.1 & 0 \\ -2.1 & 4.2 & -2.1 \\ 0 & -2.1 & 2.1 \end{bmatrix} x10^6 N/m \tag{10}$$

The damping matrix of the structure is derived by the Rayleigh damping method with the damping ratios of the first two modes assumed to be 3% of critical damping [20]. The mass, stiffness and damping matrices, **M**, **K** and $\mathbf{C}_{damp}$, are used to calculate the system matrix, $\mathbf{A} \in R^{6x6}$. With the MR damper installed at the base of the structure, the actuator location matrix, $\mathbf{B} \in R^{6x1}$, is formulated as $\mathbf{B} = [0 \ 0 \ 0 \ 1/6000 \ 0 \ 0]^T$. Similarly, the location matrix of the applied seismic lateral force, $\mathbf{H} \in R^{6x1}$, is derived as $\mathbf{H} = [0 \ 0 \ 0 \ -1 \ -1 \ -1]^T$.

Two LQR control solutions are formulated to minimize two different response parameters. First, the displacement and velocity response of each floor relative to the base of the structure is minimized:

$$\mathbf{C}_1 = \begin{bmatrix} I & 0 \\ 0 & 10I \end{bmatrix}_{6x6} \tag{11}$$

The LQR control gain, $\mathbf{G}_1 \in R^{1x6}$, that minimizes the relative displacement and velocity of each floor is found by minimization of the cost function:

$$J = \int_0^{t_f} \mathbf{z}^T \mathbf{C}_1{}^T \mathbf{C}_1 \mathbf{z} + \mathbf{u}^T \mathbf{R} \mathbf{u} \tag{12}$$

where $\mathbf{C}_1{}^T\mathbf{C}_1$ and **R** are both positive definite matrices that ensure the cost function can be minimized. A second LQR gain matrix, $\mathbf{G}_2$, is formulated to minimize the inter-story drift of the structure by selection of the following **C** matrix:

$$\mathbf{C}_2 = \begin{bmatrix} 1 & 0 & 0 & 0 & 0 & 0 \\ -1 & 1 & 0 & 0 & 0 & 0 \\ 0 & -1 & 1 & 0 & 0 & 0 \end{bmatrix} \tag{13}$$

The LQR control solutions, as presented above, are formulated in the continuous-time domain. However, the wireless control system will operate in the discrete-time domain by commanding the MR damper on a fixed time interval, Δt, where $t = k\Delta t$:

$$u_{MR}(k) = \mathbf{G}_d \mathbf{z}(k) \tag{14}$$

The equivalent gain matrix in the discrete-time domain, $\mathbf{G}_d$, is determined by discretizing the continuous-time system using the sample time step and zero-order hold (ZOH) approximations.

4.2. Communication scheme for wireless control system

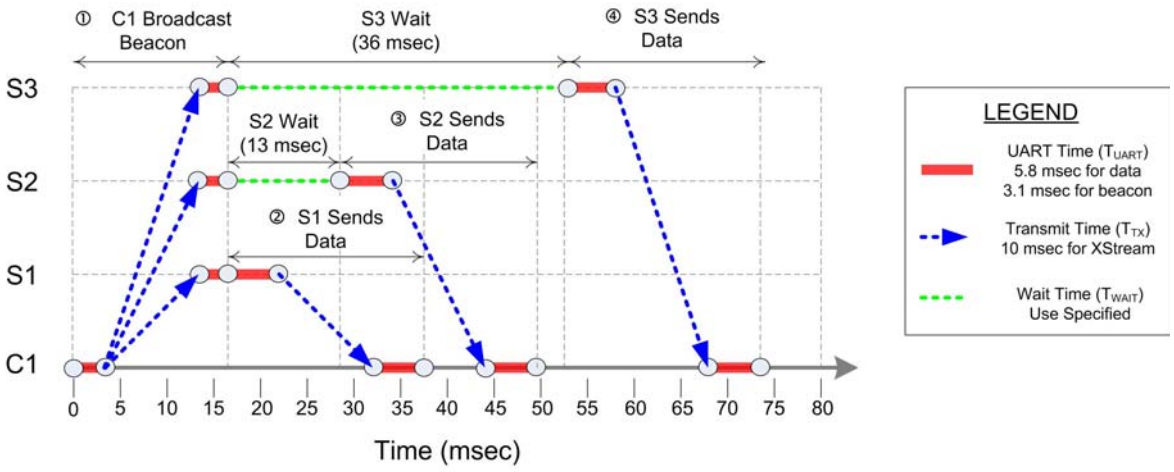

Figure 3. Timing diagram detailing the medium access control scheme of the wireless control system

To maximize the effectiveness of the control system, the smallest possible discrete-time sample time, Δt, is desired. For the wireless control system, the sample time will depend upon the time needed for the reliable exchange of data between the wireless sensors. Since all of the wireless sensors share the 2.4 GHz wireless channel, a reliable medium access control (MAC) scheme must be implemented to ensure no two sensors contend for the bandwidth at the same time. Contention for the limited bandwidth would adversely effect the reliability of the wireless communications resulting in data loss.

In the wireless control system, wireless sensor C1 is the central system node responsible for: (1) keeping time, (2) collecting state data from wireless sensors S1, S2 and S3, (3) calculating optimal control force to be generated, and (4) issuing commands to the MR damper. Wireless sensor C1 is designed to be the centralized coordinator of the entire wireless control system. At each time step, wireless sensor C1 broadcasts a wireless beacon signal asking each wireless sensor to report its measurement data. Upon receipt of the beacon signal, wireless sensor S1 sends its sensor data to the wireless sensor C1. Simultaneously, wireless sensors S2 and S3 remain idle for a period of time to allow the exchange of data between S1 and C1 to complete. After a short time period, wireless sensor S2 establishes communication with C1 to transfer its state data. Shortly after this transfer, wireless sensor S3 communicates its state data to C1. This approach effectively divides the sample time window into small segments with each communication step provided exclusive access to the wireless medium. As shown in Figure 3, this time division multiple access (TDMA) MAC scheme ensures no two radios attempt to communicate their data to wireless sensor C1 at the same time.

Prior to installation in the test structure, the timing of the TDMA MAC scheme is optimized to be as fast as possible. In optimizing the MAC scheme, the time needed for the exchange of data between two wireless sensors is measured in the laboratory. The peer-to-peer communication time is dependent upon the size of the data packet used to transmit data. For example, the initial beacon signal generated by wireless sensor C1 is 6 bytes long while the packets transmitting data from sensors S1, S2 and S3 are 11 bytes; as a result, data packets take longer to communicate than beacon packets. The time needed to transfer each wireless packet is broken down to three parts. First, the time needed by a transmitting radio to receive a packet via a serial port from the wireless sensor microcontroller is measured to be 3.1 and 5.8 msec for the beacon and data packets, respectively. This time is a function of the speed of the universal

asynchronous receiver/transmitter (UART) serial port (19,200 bits per second). The second part is the time for the modulation of the packet upon the wireless channel; irrespective of the packet size, this time is measured to be 10 msec. The last part is the time needed by the radio to send the wireless packet received to the microcontroller via the serial port. This time is identical to the time it takes to communicate the same packet on the serial port: 3.1 msec for the beacon packet and 5.8 msec for the data packet.

The total time needed to complete the transmission of the beacon signal from the microcontroller of C1 to the microcontroller of S1, S2 and S3 is 16.2 msec. After receipt of the beacon signal, wireless sensor S1 immediately initiates its communication lasting 21.6 msec while wireless sensor S2 and S3 back off for 13 and 36 msec, respectively. At precisely 13 msec after receiving the beacon signal, wireless sensor S2 wirelessly transmits its state data. Similarly, 36 msec after receiving the beacon signal, wireless sensor S3 sends its data to C1. The entirety of the exchange of data takes 74 msec. Simultaneous to the receipt of state data, wireless sensor C1 is making the appropriate calculations to determine the control signal to be applied to the MR damper. Including the time needed to determine the optimal control action, the total time step for the wireless control system is set to Δt = 0.08 sec (12.5 Hz).

4.3. Embedded software for determination of MR damper command

The embedded software that automates the wireless control system is written in a modular fashion to provide flexibility in the implementation of the control solutions. The first computational module of the embedded software calculates the optimal control force to be applied by the MR damper using response data measured by the wireless control system. When velocity sensors are interfaced to the wireless sensors, half of the state response of the system is measured. For example, the velocity meter installed on the i^{th} floor provides a measurement of the absolute velocity, v_i, allowing the relative velocity components of the state to be determined: $\dot{\mathbf{x}}(k) = \{v_1\text{-}v_0 \;\; v_2\text{-}v_0 \;\; v_3\text{-}v_0\}^T$. To simplify the calculation of the LQR control force, the displacement components of the state are ignored: $\mathbf{z}(k) = \{0\ 0\ 0 \;\; \dot{\mathbf{x}}(k)\}^T$. Using the truncated state, the desired control force to be applied by the MR damper, $u_{MR}(k)$, is calculated by Equation 14 using the LQR gain matrices ($\mathbf{G}_{d1}$ or $\mathbf{G}_{d2}$). Execution of this equation by the wireless sensor consists only of the multiplication and addition of floating point numbers and takes fractions of a millisecond to complete. Should a velocity reading not be received by wireless sensor C1 within the allotted time window of the TDMA communication scheme, the absolute velocity of that floor is designated as zero for that time step, $v_i = 0$.

In practice, structural control systems employ accelerometers to measure the dynamic structural response. However, feedback of accelerations require additional processing at the controller. Specifically, Kalman estimators are needed to estimate the state response of the structure. If the equation describing the dynamic equilibrium of the structure is written in its discretized form:

$$\mathbf{z}(k+1) = \mathbf{\Phi}\mathbf{z}(k) + \mathbf{\Gamma}u_{MR}(k)$$
$$\mathbf{y}(k) = \begin{Bmatrix} \ddot{x}_1 \\ \ddot{x}_2 \\ \ddot{x}_3 \end{Bmatrix} = \begin{bmatrix} -\mathbf{M}^{-1}\mathbf{K} & -\mathbf{M}^{-1}\mathbf{C}_{damp} \end{bmatrix}\mathbf{z}(k) + [\mathbf{B}]u_{MR}(k) = \mathbf{C}\mathbf{z}(k) + \mathbf{D}u_{MR}(k) \qquad (15)$$

then the measured state response, $\mathbf{y}$(k), can be stated as the vector of accelerations of each degree-of-freedom of the structure, $\ddot{x}_i$, relative to the base. The steady-state Kalman estimator is determined so that the full state at step *k+1* can be estimated:

$$\hat{\mathbf{z}}(k+1) = (\mathbf{\Phi} - \mathbf{LC} + \mathbf{\Gamma G} - \mathbf{LDG})\hat{\mathbf{z}}(k) + \mathbf{Ly}(k) \quad (16)$$

where the estimated state, $\hat{\mathbf{z}}$, is determined based on the steady-state Kalman gain matrix, **L**. The steady-state Kalman estimator is encoded in the wireless sensor so that an estimate for the full state can be made at each time-step using measured accelerations. The wireless sensor then uses the estimated state to calculate the desired control force to be applied by the MR damper: $u_{MR}(k) = \mathbf{G}_d \hat{\mathbf{z}}(k)$. Again, should a data point not be received by the wireless sensor, the measured state response, **y**(k), would have a zero in lieu of the true measured value not received.

After wireless sensor C1 calculates the control force, u_{MR}, it must then determine the appropriate command voltage that will generate the reaction force in the damper. The linearly parameterized Bouc-Wen model (Equation 5) derived for the 20 kN MR damper is coded as the last embedded software module. Prior to installation in the test structure, the Bouc-Wen model parameters, θ_i, are calculated for 11 voltage values between 0 and 1 V (0.1 V increments). A table of the 5 model parameters are stored for the 11 voltage levels. At each time step, the relative velocity of the first story, $\dot{x}(k)$, and the hysteretic restoring force of the damper, $z(k)$, are used to calculate the MR damper force, $F(k+1)$, that correspond to each voltage level. The 11 values for $F(k+1)$ are then compared to the desired control force, $u_{MR}(k)$; the force closest to the desired control force is noted and the corresponding voltage applied. The final step is to update the hysteretic restoring force, $z(k+1)$ which is saved by the wireless sensor for the next time step.

5. VALIDATION OF THE WIRELESS CONTROL SYSTEM

To assess the performance of the wireless control system, three earthquake excitations are selected for application to the test structure by the shaking table. Horizontal acceleration time-history records corresponding to the 1940 El Centro (Imperial Valley Irrigation District Station, North-South), 1999 Chi-Chi (TCU-076 Station, North-South) and 1995 Kobe (JMA Station, North-South) earthquakes are selected. The El Centro ground motion record is a far-field record whereas the Chi-Chi and Kobe records are near-field records. The absolute peak acceleration recorded for these three earthquakes are 3.42, 4.20, and 8.18 m/s^2, respectively. However, to keep the test structure in its linear elastic regime, the peak absolute accelerations of the El Centro, Chi-Chi and Kobe ground motion records are scaled to 1, 0.9 and 0.85 m/s^2, respectively.

Combined with the different sensing transducers utilized by the wireless monitoring system (velocity meters versus accelerometers) and the different gain matrices derived ($\mathbf{G}_{d1}$ and $\mathbf{G}_{d2}$) , a total of 8 unique tests are conducted to assess the performance of the wireless control system. In addition, the same ground excitations are applied to the structure with the damper fixed to its minimum and maximum damping coefficients (0 and 1 V, respectively). The response of the structure using the wireless feedback control

Table 1. Overview of the experimental tests conducted to assess the efficacy of the wireless control system

	Passive Control		Velocity Feedback		Acceleration Feedback	
Earthquake Record	0 V	1 V	$\mathbf{G}_{d1}$	$\mathbf{G}_{d2}$	$\mathbf{G}_{d1}$	$\mathbf{G}_{d2}$
El Centro NS (Imperial)	Test 1	Test 2	Test 7	Test 10	Test 11	Test 14
Chi-Chi NS (TCU-076)	Test 3	Test 4	Test 8	-	Test 12	-
Kobe NS (JMA)	Test 5	Test 6	Test 9	-	Test 13	-

system will be compared to the damper configured in its passive setting. Table 1 summarizes the 14 tests that are used to assess the performance of the wireless control system.

In addition to the tests conducted by the wireless monitoring system, the tethered laboratory data acquisition system is also used to perform real-time feedback control of the test structure. Again, the structure is controlled by the tethered system using both velocity meters and accelerometers. Since communication in the tethered system is performed using coaxial wiring, the tethered control system can operate using a much higher sample rate. The tethered monitoring system employs a sample rate of 200 Hz which is an order of magnitude faster than the 12.5 Hz sample rate of the wireless control system.

For all of the closed-loop control tests performed, three evaluation criteria will be considered. First, the absolute maximum inter-story drift will be calculated for each floor of the structure. Second, the peak acceleration of each floor, relative to the base, will be evaluated. The last metric for assessing the effectiveness of the closed-loop control system will be a scalar cost function looking at the total kinetic and strain energy experienced by the structure over the duration of the base excitation:

$$J = \sum_{k} \mathbf{z}(k)^{T} \begin{bmatrix} \mathbf{K} & 0 \\ 0 & \mathbf{M} \end{bmatrix} \mathbf{z}(k) \tag{17}$$

The cost function for each closed-loop control test, J_C, will be compared to that of the structure controlled in a passive configuration with the MR damper set to its smallest damping coefficient (0 V configuration), J_0:

$$\overline{J} = J_C / J_0 \tag{18}$$

A cost function ratio $\overline{J} < 1$ indicates the closed-loop control system outperforms the passive damper set to its minimum damping coefficient. A number greater than 1 would indicate the control system is working to the detriment of the structure.

5.1. Velocity feedback control

In total, four tests are conducted to assess the performance of the wireless control system using a velocity feedback solution. Three of the tests, Tests 7 (El Centro), 8 (Chi-Chi) and 9 (Kobe), adopt the first gain matrix, $\mathbf{G}_{d1}$, while Test 10 (El Centro) adopts the second gain matrix, $\mathbf{G}_{d2}$. Recall, $\mathbf{G}_{d1}$ is designed to minimize (regulate) the displacement and velocity of each floor relative to the base; similarly, $\mathbf{G}_{d2}$ is designed to minimize inter-story drifts. Consider Test 7 with the El Centro NS ground motion applied to the structure while the wireless control system mitigates the structural response. Figure 4 presents the corresponding velocity response of the structure at the top-most story (3rd floor). As can be seen, the response measured by the velocity meter interfaced to the wireless sensor S3 is identical to that recorded by the laboratory data acquisition system using a separate velocity meter. The time history records recorded at other degrees-of-freedom also reveal the response measured by wireless sensors (S2 and S1) to be identical to that recorded by the tethered data acquisition system. It should be noted that the greatest response in the structure occurs from roughly 5 to 15 seconds during which time the ground motion attains its peak absolute value (0.1 g at 7.28 sec). The displacement response of the controlled structure during Test 7, as measured by the laboratory tethered data acquisition system, is presented in Figure 5. The displacement response of the controlled structure using the wireless structural control system is superimposed upon the displacement response recorded when the MR damper is set to its minimum (0 V)

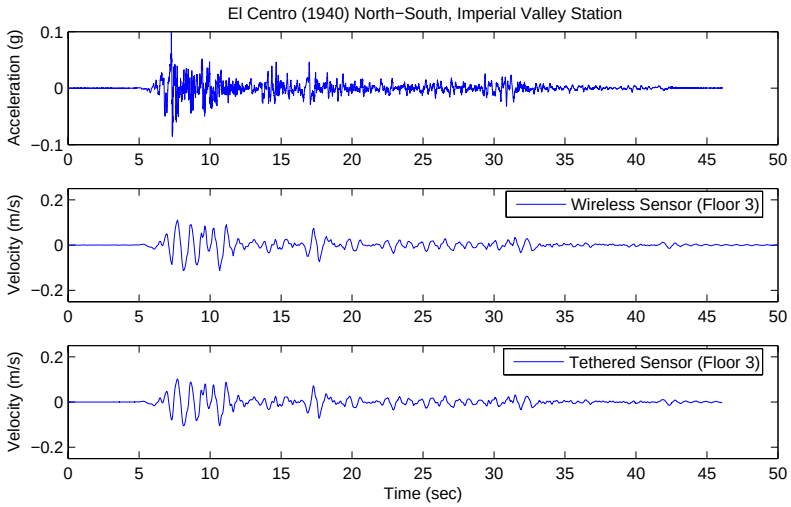

Figure 4. Velocity response of the 3rd story of the test structure under the El Centro NS ground motion: (top) applied ground acceleration, and the velocity measured by the (middle) wireless and (bottom) tethered sensors.

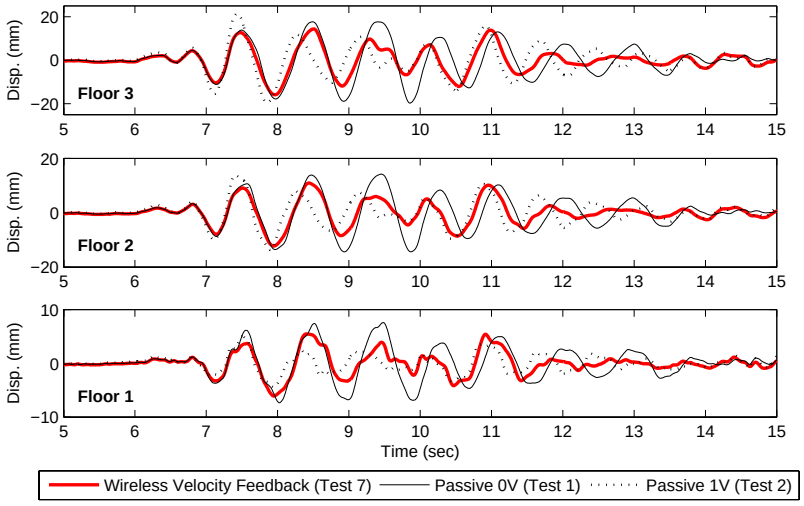

Figure 5. Segment of structural displacement response time histories when controlled (wireless velocity feedback and minimum and maximum passive damping) during El Centro NS ground motion: (top) floor 3, (middle) floor 2, and (bottom) floor 1.

and maximum (1 V) damping coefficients. The response of the structure, during the interval of greatest response (5 to 15 sec), is clearly reduced by the velocity feedback wireless control system compared to when the damper is fixed at the minimum and maximum damping coefficients. Similar observations can be made for all of the structure's three stories.

At each time step, wireless sensor C1 uses the measured velocity of each floor to calculate the LQR control force (Equation 14). The modified Bouc-Wen model is then used to determine the command

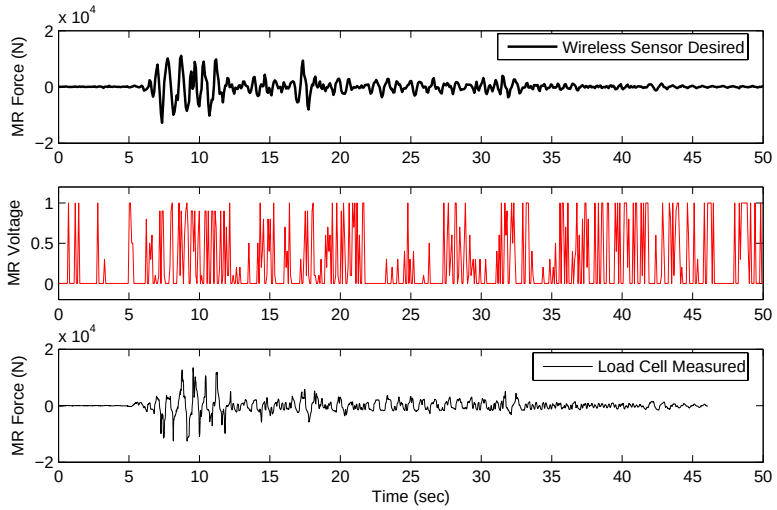

Figure 6. MR damper control force: (top) desired control force calculated, (middle) the voltage command signal issued to the MR damper by the wireless sensor, and (bottom) actual control force measured by the load cell.

voltage to be applied to the MR damper by the wireless sensor. Using the load cell installed in series with the MR damper (see Figure 2), the true force applied by the MR damper is measured by the laboratory tethered data acquisition system. As presented in Figure 6, the measured MR damper reaction force and the desired control force are in strong agreement during Test 7. This agreement suggests the modified Bouc-Wen model is sufficiently accurate for determining command voltages of the MR damper to attain a desired control force in the damper. Also presented in Figure 6 is the command voltage time history issued by wireless sensor C1 during the experiment.

Plots corresponding to the maximum absolute inter-story drift and peak relative acceleration of each degree-of-freedom of the test structure are presented in Figure 7. The performance of the wireless control system is compared to the same response parameters attained when the MR damper is set to minimum and maximum damping coefficients. In addition, the maximum absolute inter-story drift and peak accelerations attained when using an LQR velocity feedback control solution implemented using the laboratory data acquisition system are superimposed upon the plots of Figure 7. It should be noted that the LQR gain matrix used with the tethered control system is derived for the higher sample rate (200 Hz) using the same response criteria ($\mathbf{C}_1$ and $\mathbf{C}_2$) as the wireless control system. As can be seen for Test 7 (El Centro), the wireless and tethered control system are both effective in reducing the inter-story drift and relative acceleration of the 2nd and 3rd stories of the structure. Both control systems outperform the cases when the MR damper is set to a passive state. However, the performance of the wireless control system is not as impressive when the two near field earthquakes, the Chi-Chi and Kobe ground motions, are applied to the structure. For both Test 8 (Chi-Chi NS) and 9 (Kobe NS), the tethered monitoring system is effective in reducing the drift and acceleration response of the structure while the wireless control system drift and acceleration responses can be worse than during the passive MR tests. The wireless control system's low sample rate and state truncation are likely causes for its poor performance during two near-field excitations. The wired control system, operating at 200 Hz, was able to effectively reduce the structural response using the same response parameters in the LQR formulation ($\mathbf{C}_1$).

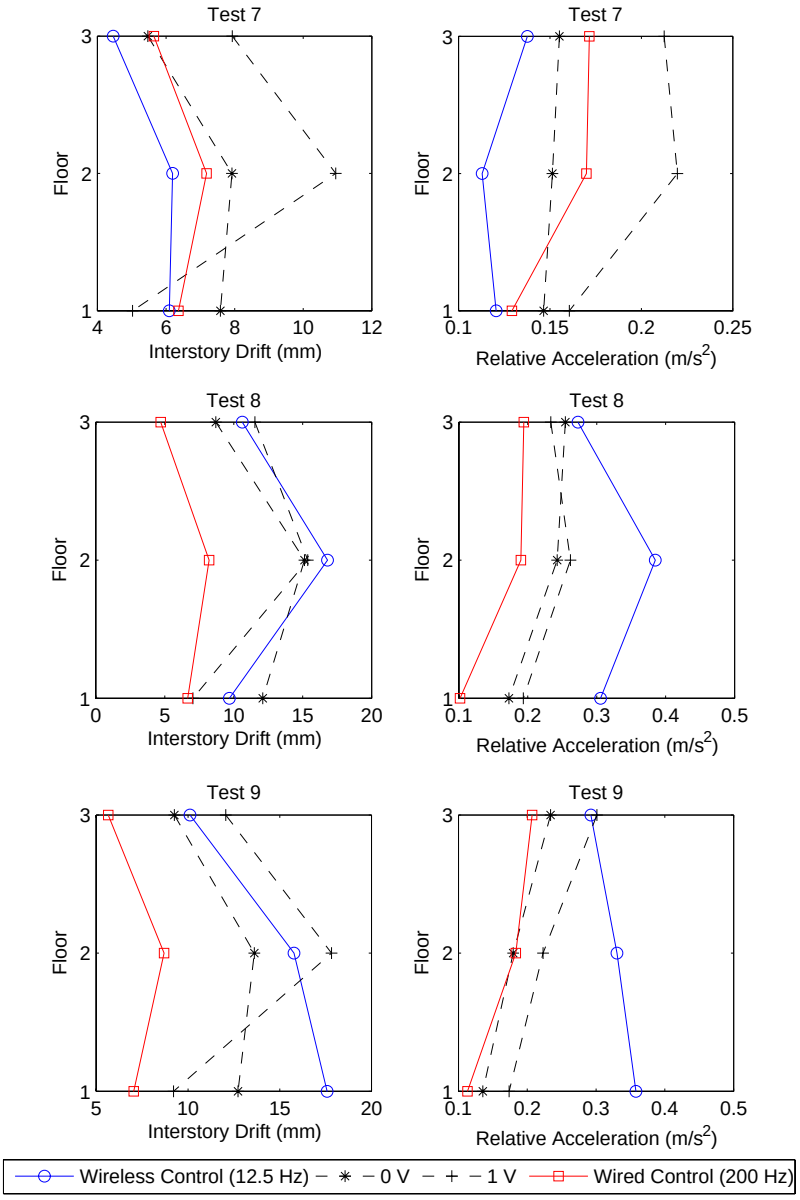

Figure 7. Maximum absolute inter-story drifts (left column) and peak acceleration relative to the base (right column) for velocity feedback control of the test structure during the El Centro (Test 7), Chi-Chi (Test 8) and Kobe (Test 9) ground motions using gain matrix $\mathbf{G}_{d1}$.

For Test 10, the LQR gain matrix corresponding to the minimization of the inter-story drift, $\mathbf{G}_{d2,}$ is employed. Again, as presented in Figure 8, the wireless control system is effective in reducing the drift and acceleration response of the structure to levels lower than those when the MR damper is operated in a passive state. Provided the same ground motion is applied during Tests 7 and 10, it is worthwile to compare the performance of the wireless control system during the two tests. The second LQR control

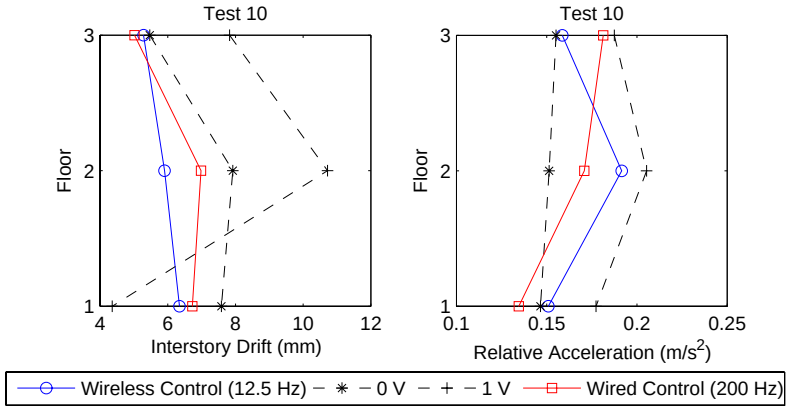

Figure 8. Maximum absolute inter-story drift (left) and peak acceleration relative to the base (right) for velocity feedback control of the test structure during the El Centro (Test 10) ground motion using gain matrix $\mathbf{G}_{d2}$.

Table 2. Performance assessment using the cost function ratio, $\bar{J}$

	Passive Control		Velocity Feedback		Acceleration Feedback	
Earthquake Record	0 V	1 V	$\mathbf{G}_{d1}$	$\mathbf{G}_{d2}$	$\mathbf{G}_{d1}$	$\mathbf{G}_{d2}$
El Centro NS (Imperial)	1	0.70	0.59	0.33	0.58	0.43
Chi-Chi NS (TCU-076)	1	1.10	0.90	-	0.59	-
Kobe NS (JMA)	1	1.40	1.07	-	0.59	-

solution ($\mathbf{G}_{d2}$) provides a marginal improvement in reducing the relative acceleration of each floor. This is expected since $\mathbf{G}_{d2}$ is designed to minimize inter-story drifts which it successfully does. However, $\mathbf{G}_{d1}$ does provide a greater reduction in the peak relative accelerations of the structure.

Plots of the maximum absolute drifts and accelerations reveal the effectiveness of the wireless control system in mitigating peak, or rather worst-case, response parameters. In contrast, the cost function ratio, $\bar{J}$, is calculated for each control experiment to assess the wireless control system effectiveness over the entire time history of the excitation. The cost function ratios for the El Centro excitations reveal the effectiveness of the wireless control system. Roughly speaking, the control system exhibits 59 and 33% of the total response energy corresponding to the structure when the minimum MR damping coefficient is set. This is in contrast to when the MR damper is set to its maximum damping coefficient where the structure exhibits 70% of the response energy compared to the minimum MR damping coefficient configuration. Consistent with the observations previously made during the Chi-Chi and Kobe excitations, the cost function ratio also reveals the wireless control system is only mildly effective in mitigating the response of the structure during the full time history of the excitation.

5.2. Acceleration feedback control

The acceleration feedback control solution is installed in wireless sensor C1. Using accelerations measured by the wireless sensors, the full state response, $\hat{\mathbf{z}}$, is estimated. Using $\mathbf{G}_{d1}$ for acceleration feedback control, the structure is exposed to the El Centro, Chi-Chi and Kobe earthquakes (Tests 11, 12 and 13, respectively). As shown in Figure 9, the wireless control system is effective in reducing the inter-story drift response of the structure under all three applied ground motions; the drift response is below those corresponding to the MR damper in a passive state (minimum and maximum damping coefficients).

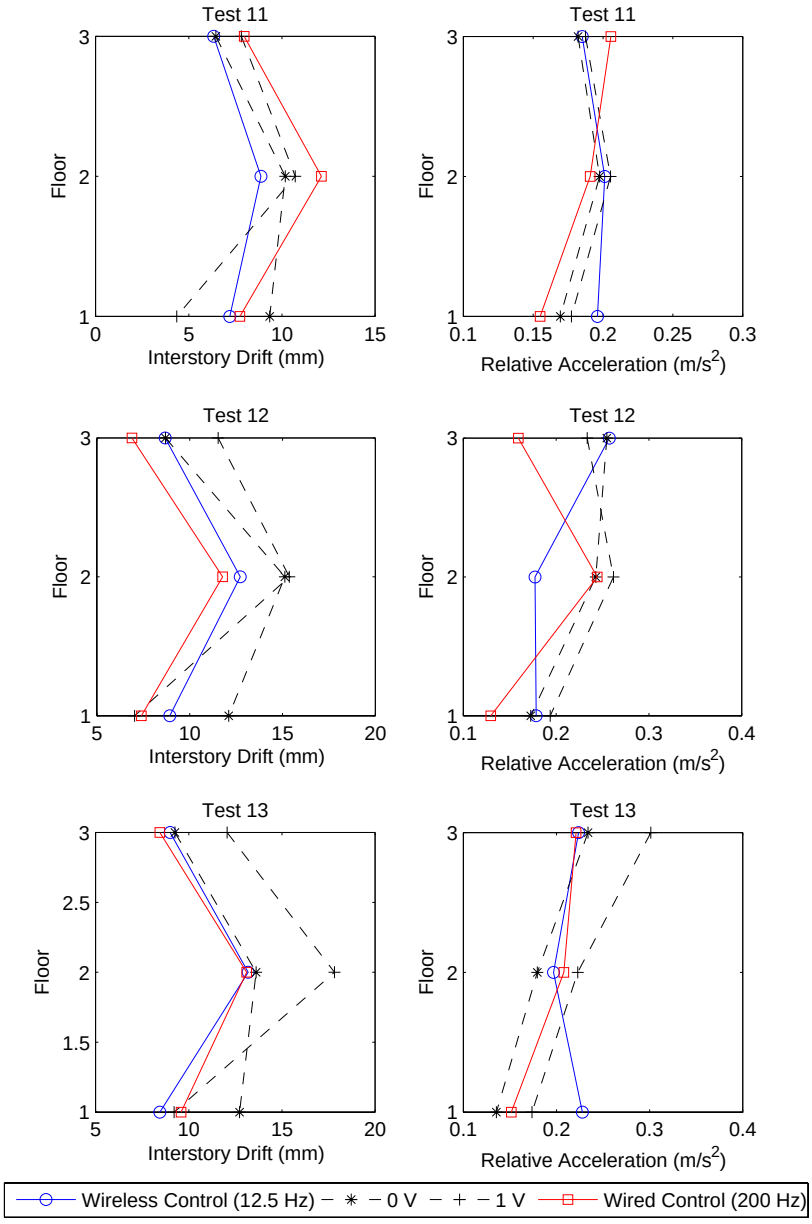

Figure 9. Maximum absolute inter-story drifts (left column) and peak acceleration relative to the base (right column) for acceleration feedback control of the test structure during the El Centro (Test 11), Chi-Chi (Test 12) and Kobe (Test 13) ground motions using gain matrix $\mathbf{G}_{d1}$.

When comparing the inter-story drift performance of the wireless control system to the wired control system, the wireless control system exhibits a superior performance. However, the wired control system exhibits a slightly better performance when considering the peak relative acceleration of each floor. The second control solution, $\mathbf{G}_{d2}$ (Test 14), allows the wireless control system to exhibit an excellent inter-

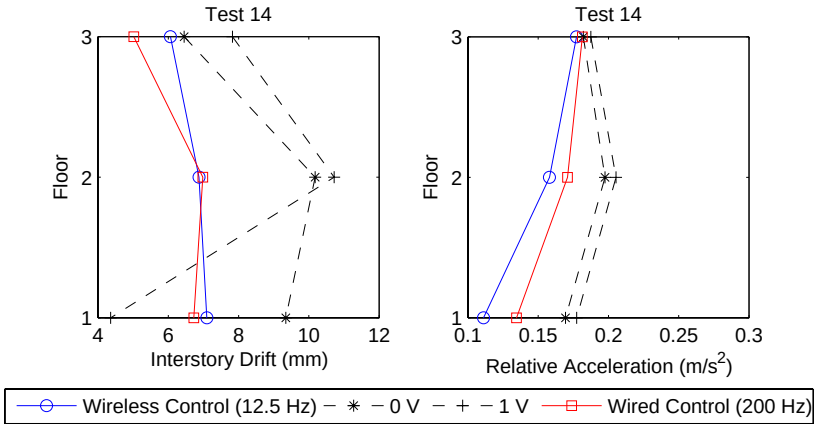

Figure 10. Maximum absolute inter-story drift (left) and peak acceleration relative to the base (right) for acceleration feedback control of the test structure during the El Centro (Test 14) ground motion using gain matrix $\mathbf{G}_{d2}$.

story drift and peak acceleration performance. As presented in Figure 10, the wireless control system is as effective as the wired control system when implementing this control solutions. For both control solutions ($\mathbf{G}_{d1}$ and $\mathbf{G}_{d2}$), the cost function ratio $\bar{J}$ reveal the wireless control system is effective over the full excitation resulting in lower response energy than when the MR damper is set to minimum and maximum damping coefficients.

5.3. Quality of the wireless communication channel

In total, 47 tests are conducted using the prototype wireless control system. During each of the closed-loop control tests, wireless sensor C1 logs the reception of data from each wireless sensor installed in the upper levels of the test structure. After the completion of each test, the data received by wireless sensor C1 is sent to a remote data server where it can be stored and analyzed. With the performance of the control system dependent upon the reliability of data delivery, the logs of received data by wireless sensor C1 are analyzed to determine how often data is lost by the wireless control system. A bar graph of the percent of data points not received by wireless sensor C1 are plotted in Figure 11. Only a handful of cases exhibit data losses of roughly 2%. However, the vast majority of the tests have data loss rates less than 1% and in many cases, less than 0.5%. For each floor, a histogram of the percentage of lost data is determined. As seen in Figure 11, the histograms reveal the data loss phenomena in the wireless control system exhibits a log-normal probability distribution function. To illustrate this distribution more clearly, a log-normal distribution is fitted to each histogram and is superimposed. The mean and standard deviations of the fitted log-normal distributions, μ and σ, are also presented on each plot. The mean data loss for floors 1, 2 and 3 are determined to be 0.43, 0.47 and 0.70%, respectively.

6. CONCLUSIONS

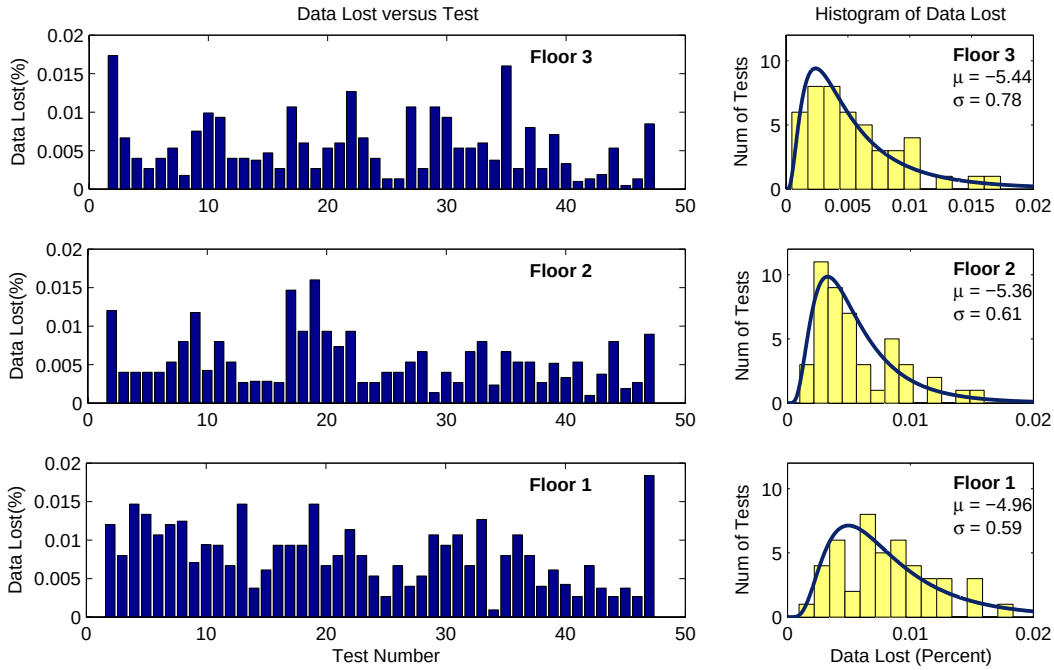

Figure 11. Quantitative assessment of the reliability of the wireless communication channel: (left column) percentage of lost data points for each floor during 47 tests, and (right column) histogram of number of tests versus percentage of data loss with fitted log-normal probabilistic distribution functions.

As semi-active control devices grow in popularity and decrease in cost, large-scale control systems defined by high actuation densities emerge. As the nodal density of control systems increase, additional coaxial wire is needed for communication between sensors, actuators and a centralized controller. To eradicate the need for expensive wiring, wireless sensors are proposed for the design of closed-loop structural control systems. A low-cost wireless sensor prototype capable of assuming all of the tasks associated with operating a structural control system has been proposed. Namely, the wireless sensor is designed to collect sensor data with high precision, calculate desired control forces, and issue command signals to control devices. A significant portion of the wireless sensor design is the embedded software that automates the operation of the unattended wireless sensors. To achieve a high level of performance, the embedded software is written to ensure reliable transfer of state data between wireless sensors at each time step. Due to the time necessary for the reliable transfer of data between the wireless sensors and the calculation of the MR damper command signal, the wireless control system is able to operate at 12.5 Hz.

To validate the performance of the wireless structural control system, a 4 node wireless sensor network is installed within a full-scale three-story steel structure mounted to a shaking table. At the base of the structure is a 20 kN MR damper that is used to mitigate the response of the structure during application of ground motions. The wireless control system proves effective in reducing the inter-story drifts and relative acceleration of each floor during seismic excitation. Two sensing transducer types are adopted by the wireless control system: velocity transducers and accelerometers. When velocity meters are interfaced to the wireless sensors, the control system is able to mitigate structural responses to levels below the structural response with the damper fixed at its maximum damping coefficient for the El Centro NS ground motion. However, when the Chi-Chi NS and Kobe NS near-field ground motion records are

applied to the structure, the wireless control system is only mildly effective in reducing the total strain and kinetic energy response of the structure. This could be the result of the suboptimal nature of the truncated gain matrix in combination with the low sample rate of the wireless system (12.5 Hz). During a second set of tests, accelerometers are adopted because they represent a more widely used transducer for structural monitoring. Irrespective of the ground motion applied, the acceleration-feedback control solution was proven effective in the reduction of peak inter-story drifts and relative accelerations. During operation, the wireless control system's wireless communication channel proved highly reliable with minimal data loss (< 2%) occurring during the tests.

In conclusion, the general success of the wireless control system presented herein suggests wireless sensor networks are a promising technology capable of operation within a real-time control system. However, additional research is needed to further advance wireless sensors for real-time feedback control of civil structures. The current wireless control system operates at a relatively slow speed compared to commercial tethered control systems. The 12.5 Hz sample rate is largely governed by the time necessary to carry out calculations by the wireless sensors in addition to a conservative TDMA communication protocol. Current research efforts are exploring improvements in the hardware design of the wireless sensor prototype to include more computationally powerful microcontrollers (to speed up the computational overhead) and faster wireless modems. It should be noted that the current implementation of the wireless control system employs a modest number of nodes. As the wireless control system grows, issues such as data loss in the wireless communication channel and time for data collection increase faster than at a linear rate. As a result, decentralized control system architectures are attractive candidates for future systems designed using low-cost wireless sensor networks.

ACKNOWLEDGMENTS

This research is partially funded by the National Science Foundation under Grants CMS-0421180 and CMS-0528867 and the Office of Naval Research (ONR) Young Investigator Program. Additional support was provided by the National Center for Research on Earthquake Engineering (NCREE), the National Science Council of Taiwan, and the University of Michigan Rackham Grant and Fellowship Program. Mr. Yang Wang is supported by the Stanford Graduate Fellowship at Stanford University. The authors would like to express extreme gratitude to Prof. Kincho H. Law of Stanford University who has provided invaluable expertise in all facets of this research project.

REFERENCES

[1] Yao JTP. Concept of structural control. *Journal of Structural Division* 1972; **98**(7):1567-1574.

[2] Spencer BF and Nagarajaiah S. State of the art of structural control. *Journal of Structural Engineering* 2003; **129**(7):845-856.

[3] Kobori T, Takahashi M, Nasu T, Niwa N and Ogasawara K. Seismic response controlled structure with active variable stiffness system. *Earthquake Engineering and Structural Dynamics* 1993; **22**(11):925-941.

[4] Kurata N, Kobori T, Takahashi M, Niwa N and Midorikawa H. Actual seismic response controlled building with semi-active damper system. *Earthquake Engineering and Structural Dynamics* 1999; **28**(11):1427-1447.

[5] Gavin HP. Design method for high-force electrorheological dampers. *Smart Materials and Structures* 1998; **7**(5):664-673.

[6] Jung HJ, Spencer BF, Ni YQ and Lee IW. State-of-the-art of semiactive control systems using mr fluid dampers in civil engineering applications. *Structural Engineering and Mechanics* 2004; **17**(3-4):493-526.
[7] Symans MD and Constantinou MC. Semi-active control systems for seismic protection of structures: A state-of-the-art review. *Engineering Structures* 1999; **21**(6):469-487.
[8] Celebi M. Seismic instrumentation of buildings with emphasis on federal buildings. *Report 0-7460-68170*, United States Geological Survey, Menlo Park, CA, 2002.
[9] Lian FL, Moyne J and Tilbury DM. Network design consideration for distributed control systems. *IEEE Transactions on Control Systems Technology* 2002; **10**(2):297-307.
[10] Eker J, Cervin A and Horjel A. Distributed wireless control using bluetooth. *IFAC Conference on New Technologies for Computer Control*, 2001;
[11] Nilsson J, Bernhardsson B and Wittenmark B. Stochastic analysis and control of real-time systems with random time delays. *Automatica* 1998; **34**(1):57-64.
[12] Ploplys NJ, Kawka PA and Alleyne AG. Closed-loop control over wireless networks. *IEEE Control Systems Magazine* 2004; **24**(3):58-71.
[13] Wang Y, Lynch JP and Law KH. Design of a low-power wireless structural monitoring system for collaborative computational algorithms. *Proceedings of the SPIE - The International Society for Optical Engineering*, San Diego, CA, USA, 2005; 106-117.
[14] Lynch JP and Loh K. A summary review of wireless sensors and sensor networks for structural health monitoring. *Shock and Vibration Digest* 2006; **38**(2):91-128.
[15] Lynch JP. Design of a wireless active sensing unit for localized structural health monitoring. *Journal of Structural Control and Health Monitoring* 2004; **12**(3-4):405-423.
[16] Lin PY, Roschke P and Loh CH. System identification and real application of a smart magneto-rheological damper. *2005 IEEE International Symposium on Intelligent Control* Limassol, Cyprus, 2005; 989-994.
[17] Smyth AW, Masri SF, Chassiakos AG and Caughey TK. On-line parametric identification of mdof nonlinear hysteretic systems. *Journal of Engineering Mechanics* 1999; **125**(2):133-142.
[18] Smyth AW, Masri SF, Kosmatopoulos EB, Chassiakos AG and Caughey TK. Development of adaptive modeling techniques for non-linear hysteretic systems. *International Journal of Non-Linear Mechanics* 2002; **37**(8):1435-1451.
[19] Soong TT. *Active structural control: Theory and practice*. Longman Scientific & Technical:Essex, U.K., 1990.
[20] Chopra AK. *Dynamics of structures*. Prentice Hall:Upper Saddle River, N.J., 2001.